



SPE 121575

Viscometer for Opaque, Sealed Microemulsion Samples

Jose Lopez Salinas, Clarence A. Miller, Kuy Hun Koh Yoo, Maura Puerto, George J. Hirasaki / SPE, Rice University

Copyright 2009, Society of Petroleum Engineers

This paper was prepared for presentation at the 2009 SPE International Symposium on Oilfield Chemistry held in The Woodlands, Texas, USA, 20–22 April 2009.

This paper was selected for presentation by an SPE program committee following review of information contained in an abstract submitted by the author(s). Contents of the paper have not been reviewed by the Society of Petroleum Engineers and are subject to correction by the author(s). The material does not necessarily reflect any position of the Society of Petroleum Engineers, its officers, or members. Electronic reproduction, distribution, or storage of any part of this paper without the written consent of the Society of Petroleum Engineers is prohibited. Permission to reproduce in print is restricted to an abstract of not more than 300 words; illustrations may not be copied. The abstract must contain conspicuous acknowledgment of SPE copyright.

ABSTRACT

Formulation of surfactant EOR systems usually involves multiple salinity scans of the phase behavior of crude oil, surfactant, and brine systems. Usually, the measurements are made in sealed pipettes for accurate volume measurements without fluid loss. The volumes of oil and water solubilized into the microemulsion phase are observed to determine the optimal salinity and estimate the interfacial tension. Viscous emulsions and surfactant-rich condensed phases are not desirable. However, the only estimate of viscosity from the salinity scans is the movement (or lack of movement) of the interfaces upon tilting of the tube.

A falling-sphere viscometer with multiple, ring-shaped, inductive proximity sensors is described. The device uses 0.78 mm, gold-coated, paramagnetic, 440 stainless steel spheres. With this size sphere, it is possible to accurately estimate the viscosity of fluids from 1 to 1,200 cp. The spheres are paramagnetic, so they can be lifted to the top of the tube with a magnet, and meet the constraints of a Reynolds number less than 800 for low viscosity fluids, and a velocity fast enough to be detected for a high viscosity fluid. A data acquisition system control a set of four sensors for signal conditioning and time recording. When the same phase spans the space between a pair of sensors, its viscosity can be estimated directly from the transit time of the sphere. When two or three phases span the space between a pair of sensors, the viscosity of the undetermined phase can be estimated from the transit time across it after correcting for the transit times across the upper and/or lower phases. Thus the viscosity of a middle-phase microemulsion can be estimated even if it spans only a small fraction of the distance between sensors.

The system has been used to measure viscosities of lower-, middle-, and upper-phase microemulsions at ambient temperature. Also, apparent viscosities of macroemulsions and of the “colloidal dispersion” layer at the top of a lower-phase microemulsion have been measured.

INTRODUCTION

Salinity scan tests are used to measure phase volumes and viscosities. Designing surfactant systems for EOR usually involves multiple tests of salinity scans to determine the phase behavior of crude oil, surfactant, and brine. These measurements are frequently made in sealed pipettes for accurate volume measurements without fluid loss. From the volume of oil and water solubilized into the microemulsion phase, the optimal salinity is determined and the interfacial tension is estimated. Viscous emulsions and condensed, surfactant-rich condensed phases are not desirable. However, viscosities of the phases present in pipettes of the salinity scan tests in opaque crude oil systems can currently be estimated *in situ*

only by the movement (or lack of movement) of the interfaces upon tilting of the tube. We describe here an apparatus using a falling sphere to determine viscosities of multiple phases coexisting at equilibrium in a sealed pipette.

It is known that the terminal velocity of a sphere falling in a liquid can be related with the viscosity, the diameter of the sphere, the density of the fluid and the density of the sphere. Healy and Reed (1974) emphasized the importance of micellar structure maps using measurements of viscosity, electrical resistivity, and optical birefringence. However, it was necessary to isolate the phases for viscosity measurements. They recognized the presence of viscous fluids like gels, and fluids exhibiting birefringence. They also observed a considerable reduction in viscosity of those viscous systems when alcohol was added.

Detailed experiments conducted by Bennett *et al.* (1981) revealed that the local minimum in viscosity of those systems occur in the zone close to optimal conditions (i.e. point at which values of concentrations or temperature happen to give equal volumes of solubilization of oleic phase and aqueous phase in the microemulsion). Bennett *et al.* (1981) also observed two local maxima in viscosity, the first one close to the transition from Winsor Type I to Type III microemulsion, and the second close to the transition from Type III to Type II microemulsion. The same research group found that the location of the maxima in viscosity is not directly related with the transitions in other physical properties of the microemulsion like the degree of scattering, solubilization parameters of each phase, or the electrical conductivity ratio. However the local minimum in viscosity is close to optimal condition. This behavior is consistent with the results for other systems with alcohol content high enough that the Winsor I, III, II phase sequence is observed.

DESCRIPTION OF THE VISCOMETER

If the terminal velocity of a sphere falling through a Newtonian fluid, the densities of the fluid and sphere, and the diameter of the sphere are known, the drag coefficient can be estimated according with equation (1).

$$C_D = \frac{4}{3} \frac{\Delta\rho}{\rho} \left(\frac{gD_p}{U^2} \right), \dots\dots\dots (1)$$

The drag coefficient can be related with the Reynolds number up to 800, as shown in equation (2) given by Turton and Levenspiel correlation (1986) and in Fig. 1. Once the Reynolds number is obtained from solution of equation 2, the viscosity can be estimated using the Reynolds number definition (3). For Non-Newtonian fluids Chhabra (2007) reported equivalent relations and correlations for power law fluids.

$$C_D = \frac{24}{N_{Re}} \left(1 + 0.173 N_{Re}^{0.657} \right) + \frac{0.413}{1 + 16300 N_{Re}^{-1.09}}, \dots\dots\dots (2)$$

$$\mu = \rho U D_p / N_{Re}, \dots\dots\dots (3)$$

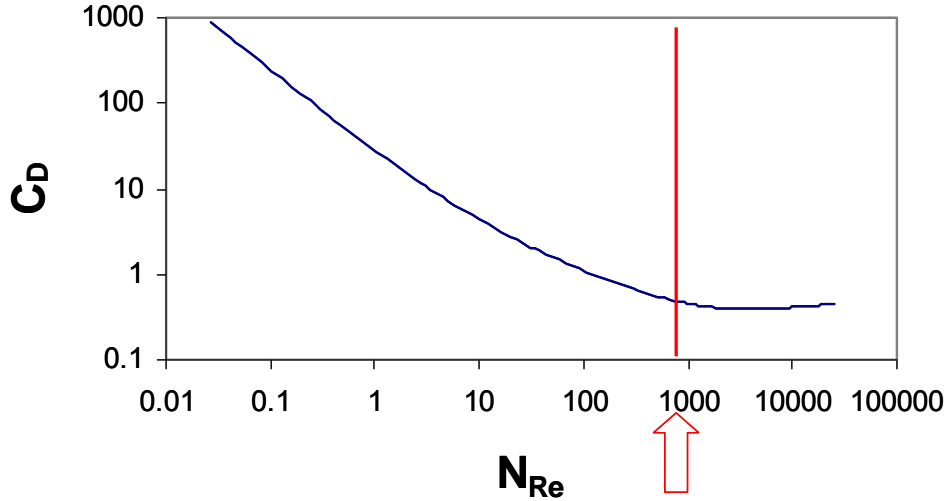


Fig.1 Drag coefficient predicted by Turton and Levenspiel (1986). The red line indicates the maximum value of Reynolds number at which viscosity can be predicted accurately.

Wall effects on the drag coefficient must be considered. Reynolds number and the ratio between particle diameter and tube (or pipette diameter) are important when this ratio exceeds 0.15 (Chhabra *et al.* 2003). The apparatus designed in this study has a ratio between diameters of 0.094. The Francis correction factor f of equation 4 is applied (Francis, 1933) for low Reynolds number ($N_{Re} < 1$). The Munroe correlation for correction factor f of equation 5 is used for higher Reynolds number (Chhabra *et al.* 2003). Calculated viscosities using these values of f were in good agreement with known viscosities for several liquids.

$$f = \left[\frac{1 - 0.475 \frac{D_p}{D}}{1 - \frac{D_p}{D}} \right]^4, \text{ for } N_{Re} < 0.1 \dots\dots\dots (4)$$

$$f = 1 - \left(\frac{D_p}{D} \right)^{3/2}, \text{ for } N_{Re} > 0.1 \dots\dots\dots (5)$$

(Note: To obtain the corrected drag coefficient, multiply drag coefficient from equation 2, by the factor f , obtained with equation 4 or 5, i.e. 1.24 or 0.97 respectively)

Inductive-ring sensors can be used to detect the location of metal spheres passing through opaque or dark samples, a situation where optical sensors fail. The paramagnetic sphere is lifted and released by a magnet located outside the pipette. The velocity of the falling sphere is estimated by measuring the time required for traveling a known distance. Different methods can be applied to trigger the timer.

The inductive-ring sensor works by generating an oscillating-electromagnetic field at resonance frequency. The inductive proximity sensor, configured as a ring produces a magnetic field that concentrates at the ring’s middle. When passing through the ring’s center, a metal sphere generates in itself eddy currents (Foucault current) which create field-loss energy that is manifested as a decrease in the amplitude of the signal measured. This reduction in amplitude is used to start or interrupt the timer (Suffi, 2000).

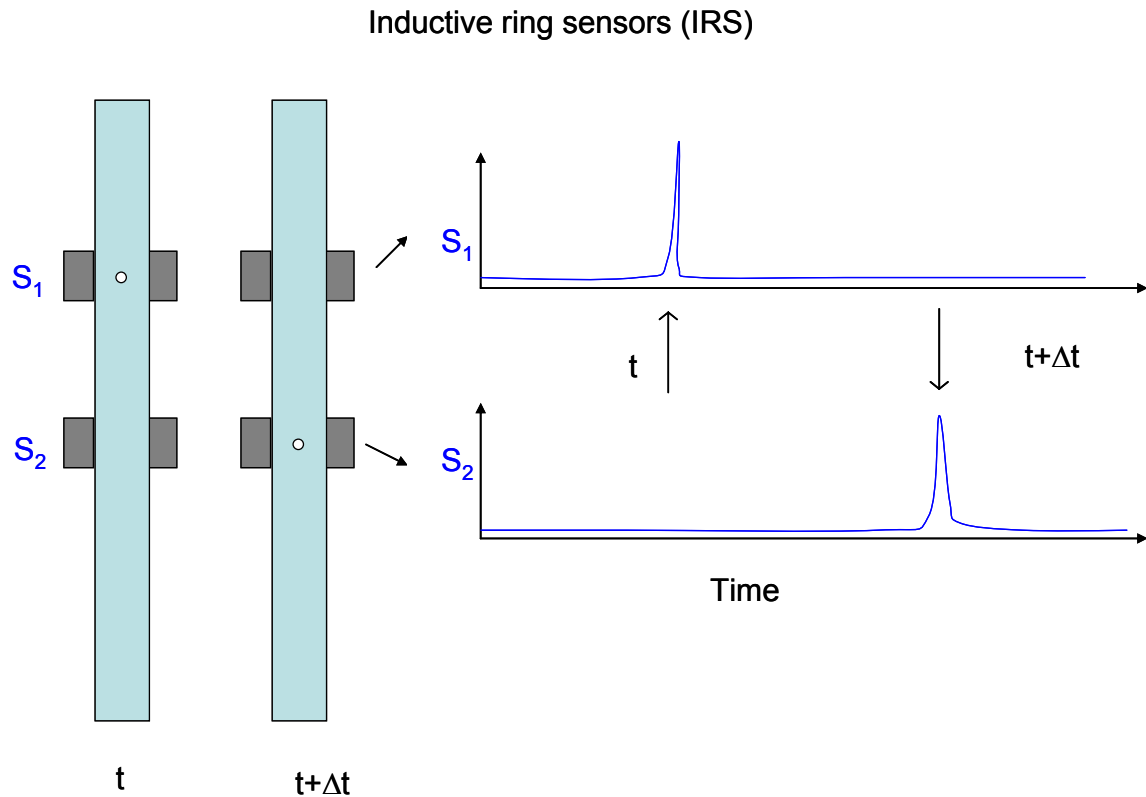


Fig.2 Illustration for sphere position at two different times. Inductive-ring sensors detect the time when the sphere passes through each sensor (the sensor sends a signal when detects decrease in signal amplitude). The transit time between sensors S_1 and S_2 is Δt , which is used to calculate terminal velocities.

A falling-sphere viscometer with four, ring-shaped, inductive proximity sensors is employed in this study. The device uses a 0.78 mm metal 440 stainless steel sphere, gold coated to prevent corrosion. Also, since the sphere is paramagnetic, it can be lifted to the top of the tube with a magnet, and can be released by removing the magnet. This size sphere meets the constraints of a Reynolds number less than 800 with water (see fig. 1) and a velocity fast enough to be detected in viscous fluids. This criterion can change when wall effects are important, according to Chhabra *et al.* (2003). A data acquisition system controls a set of four sensors for signal conditioning and time recording. When the same phase spans the space between a pair of sensors, the viscosity can be estimated directly from the transit time of the sphere. When two or three phases span the space between a pair of sensors, the viscosity of the undetermined phase can be calculated from the transit time across the undetermined phase after correcting for the transit time across the upper and/or lower phases (see Fig. 3). Thus the viscosity of a middle-phase microemulsion can be predicted even if it spans only a small fraction of the distance between sensors. The sensors are movable, but in this study all of them were set at constant separation between centers of 3.7 cm. This is the minimum spacing required to prevent interference among sensors. The transient time to reach terminal velocity should be considered when low viscosities are involved ($\mu < 1$ cp). See details of this case and additional scenarios in the Appendix.

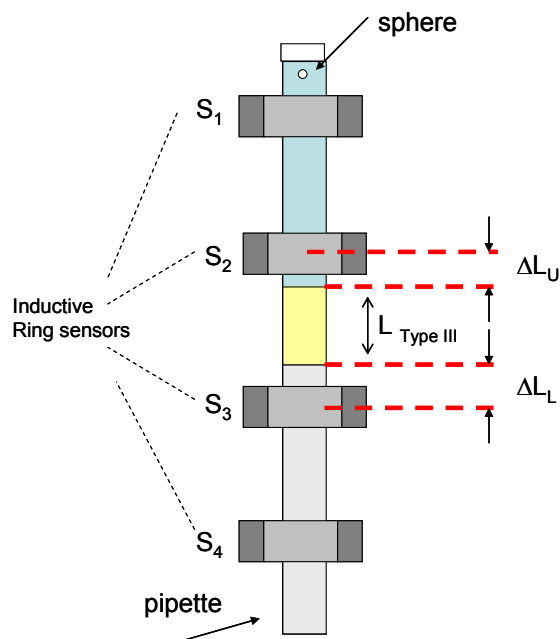


Fig.3 Illustration for location of sensors to measure viscosities of three phases in a pipette. It indicates the required distances for measuring viscosity of a middle phase microemulsion when spans a fraction of the distance between sensor S_2 and S_3 .

In the scenario shown in Fig. 3, knowing the transit time of the sphere between sensors S_1 and S_2 the viscosity of the upper phase is measured using equations 1-3. Similarly, using the transit times between S_3 and S_4 the viscosity of the lower phase is calculated. Once the viscosities of the upper phase and the lower phase are known, the transit time between S_2 and S_3 is corrected to consider only the time for passage through the middle phase. Then its viscosity is calculated.

RESULTS

Calibration and Verification

The viscosities of pure fluids, lower-, middle-, and upper-phase microemulsions and macroemulsions were determined by the falling sphere viscometer. Also, the viscosity of the “colloidal dispersion” (Liu *et al*, 2008a, 2008b) layer at the top of a lower-phase microemulsion has been measured. All the measured viscosities are apparent viscosities.

The first step in the process of measuring viscosities of the different systems was to calibrate the viscometer. The calibration was done using four different fluids with known viscosities, as indicated in Fig.4 (see Appendix for information about the fluids).

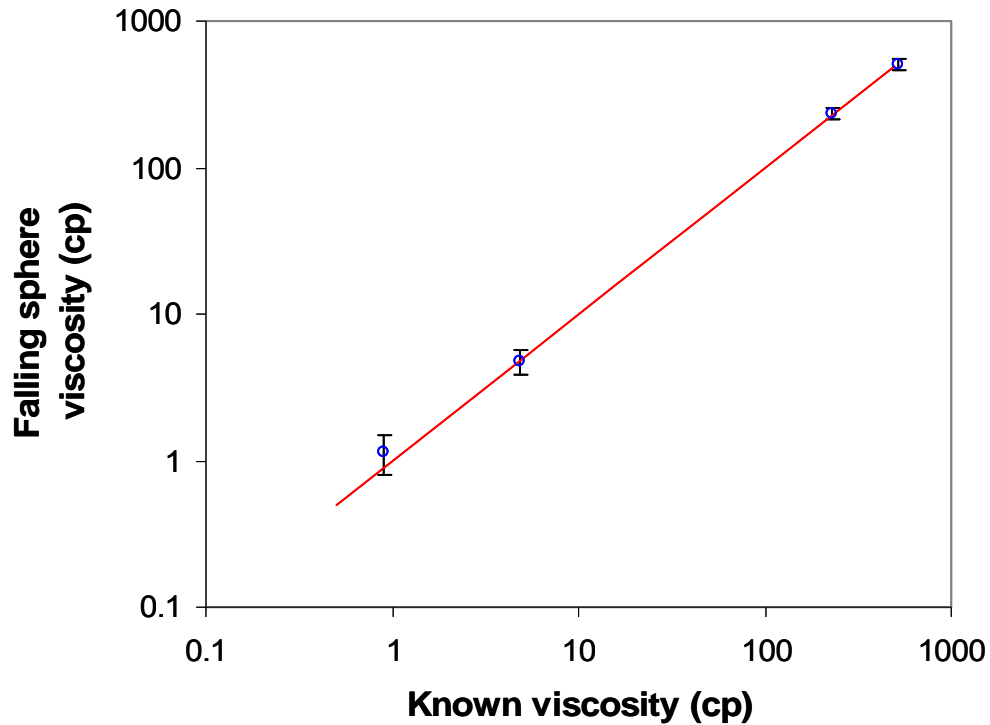


Fig.4, Verification curve for the falling sphere viscometer. Experimental viscosity values calculated with the experimental data versus the known value.

All reported viscosities are the average of at least 15 measurements per fluid, and the error bars show the precision error. The highest error is at low viscosity (less than 1 cp). Fluids with viscosity larger than 1 cp have less than 10% error with respect to the known value. The viscometer is accurate enough that no calibration adjustment was needed.

To assess the accuracy of the falling sphere viscometer, values of the viscosity of a crude oil (SMY) obtained with different viscometers were compared, as shown in TABLE 1. This crude oil, which had a density of 0.885 g/cm^3 , yielded a viscosity of 23 cp in all tested viscometers (the error among all measurement is negligible).

TABLE 1 Comparison of measurement predicted by the falling sphere viscometer vs different viscometers.

| Viscometer | Viscosity (cp) |
|---|----------------|
| Falling sphere | 23±2 |
| Brookfield (DV-III Rheometer) Strain rate 80-180 1/s | 22.4 |
| Ostwald. Cannon (IC 400-899D) | 23.0 |
| Ostwald. Cannon (IC 200-y830) | 23.9 |

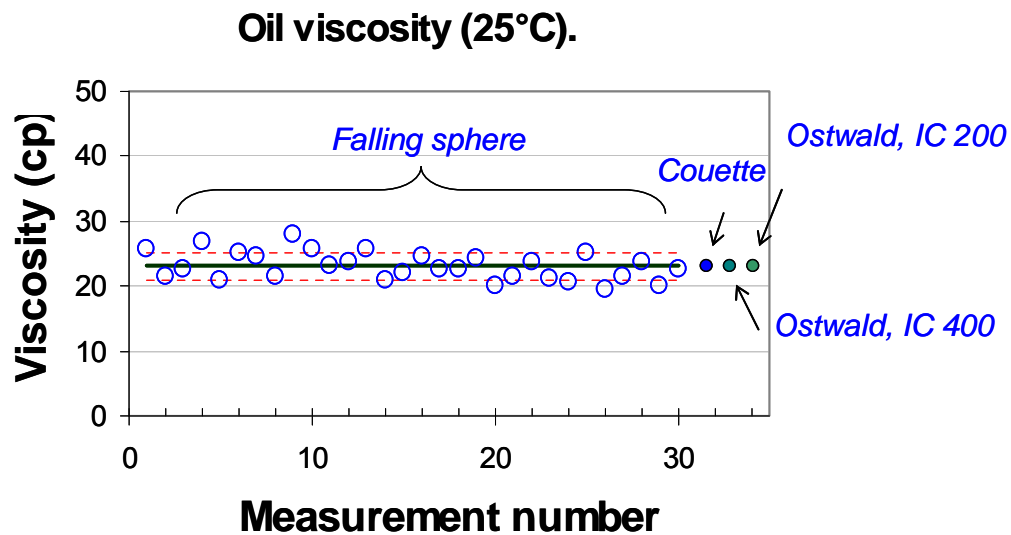


Fig.5 Test for reproducibility of the measurements give uncertainty of ± 2 cp . (\circ) Experimental data, (—) average,(- - -) standard deviation. The precision error is 9.5%. Legends indicate the viscometer used for each measurement.

Viscosity of microemulsions

After calibration of the viscometer, several multiphase systems were analyzed. The first system shown in Fig. 6 was studied to evaluate if the shape of the curve of viscosity vs salinity presented two local maxima and a local minimum, as reported by Bennett et al. (1980). That figure is a salinity scan of a mixture of a C_{12} -ortho-xylene-sulfonate (C12OXS) and tertiary amyl alcohol (tAA) in a mass ratio of 1 to 1. In this multicomponent system all the microemulsion volumes were sufficiently large to cover the entire length between adjacent sensors, so no correction was required in the viscosity determination.

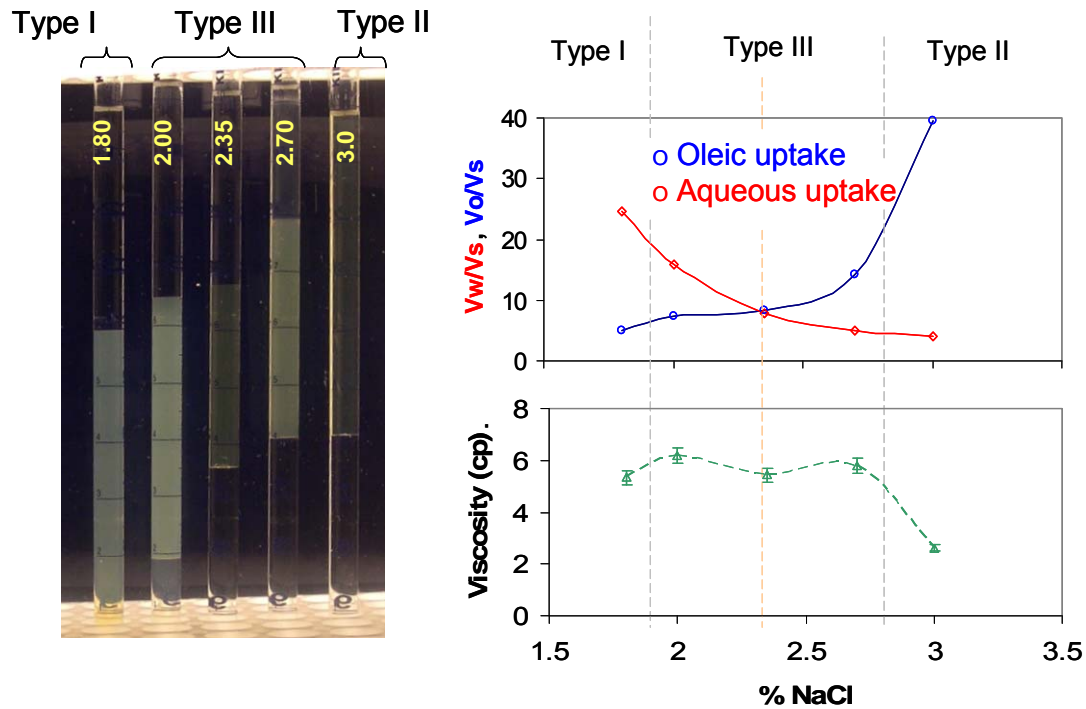


Fig.6, Salinity scan, WOR_v=1, 2% C₁₂-Ortho-Xylene-Sulfonate, 2% tertiary-Amyl Alcohol, n-dodecane. (a) At the left, in the photograph with crossed polarizers, a pattern of two local maxima and a local minimum of the visual opacity is seen, (b) At the upper right, volume of water, V_w and volume of oil, V_o, uptake per volume of surfactant, V_s, are plotted to locate optimal conditions, and (c) At the lower right, plot of the viscosity of the microemulsions. (A cross polarized filter was used for the potograph. Details of the technique are given by Benton and Miller ,1983).

The findings according with Fig. 6 are qualitatively consistent with previous observations made by Reed and Healy (1977) and Bennett *et al.* (1980, 1981) regarding visual opacity and viscosity at increasing salinity, presenting two local maxima and a local minimum. Bennett *et al.* (1980) emphasized that this behavior was an indicator of at least three microstructural regimes. The values of viscosity reported in this figure are assuming the microemulsions are Newtonian fluids. Hackett and Miller (1988) reported middle phase microemulsions systems with Newtonian behavior, and Bennett found that microemulsions are strictly Newtonian close to optimal conditions. The visusal opacity in the microemulsion in our system increased near the transitions between Winsor types, and decreased close to the optimal salinity.

Systems that present high viscosity in the middle phase

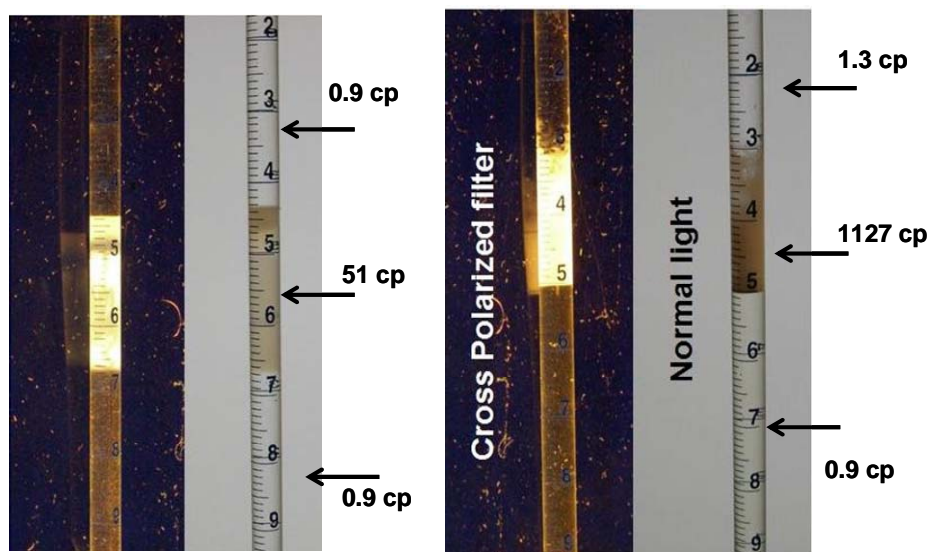


Fig.7 Systems with high viscosities a) $n\text{-C}_6$, $\text{C}_{16-17}\text{-7PO-SO}_4\text{Na}$, 0.9% Na_2CO_3 . b) $n\text{-C}_{12}$, Amine ethoxylated surfactant (A cross polarized filter was used for the photograph to detect birefringence)

The Fig. 7 depicts two cases of middle phases with high viscosity, both exhibited birefringence. The transient effect to reach terminal velocity in the middle phases is negligible because of their high viscosities. Their volumes were large enough that no correction was required in the determination of the viscosities.

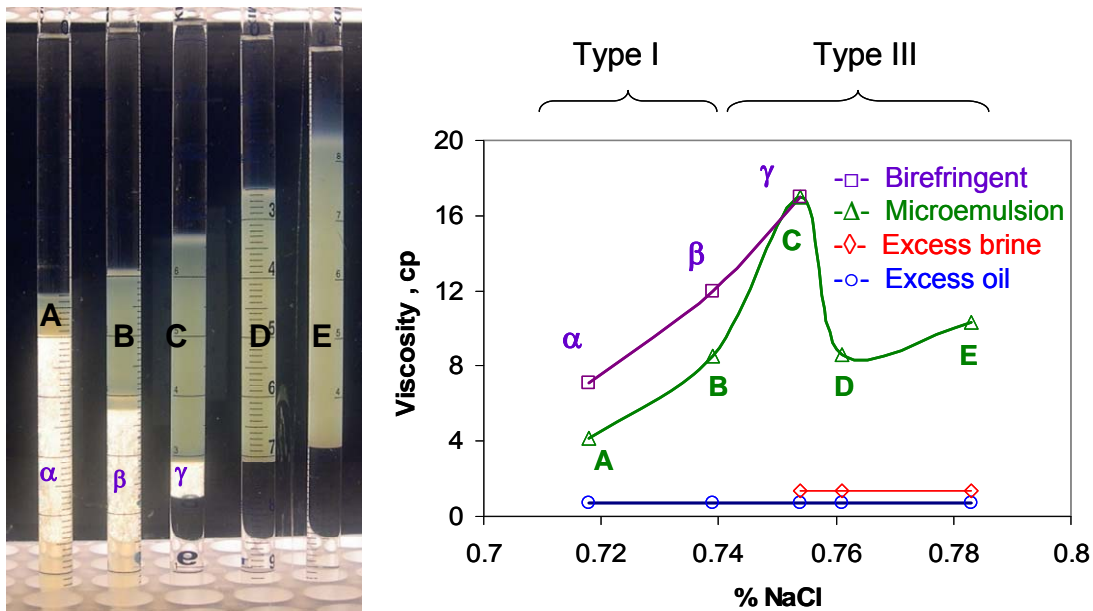


Fig.8 Viscosity of different phases in a salinity scan. Phases identified by measuring birefringence and viscosity. $WOR_v=1$, 2% C_{12} -Ortho-Xylene-Sulfonate, 1% 1-pentanol, n-dodecane. (A cross polarized filter was used for the photograph)

Fig. 8 depicts, on the right, a viscosity map of the different phases present in a salinity scan when the ratio of alcohol to surfactant is low (2:1). This map reveals a local minimum in the viscosity of the microemulsion near the composition of pipette D on the left, which is itself near optimal salinity. At low concentration of sodium chloride, the middle phase is made of a microemulsion phase in equilibrium with a phase exhibiting birefringence. This phase presented birefringence with high viscosity.

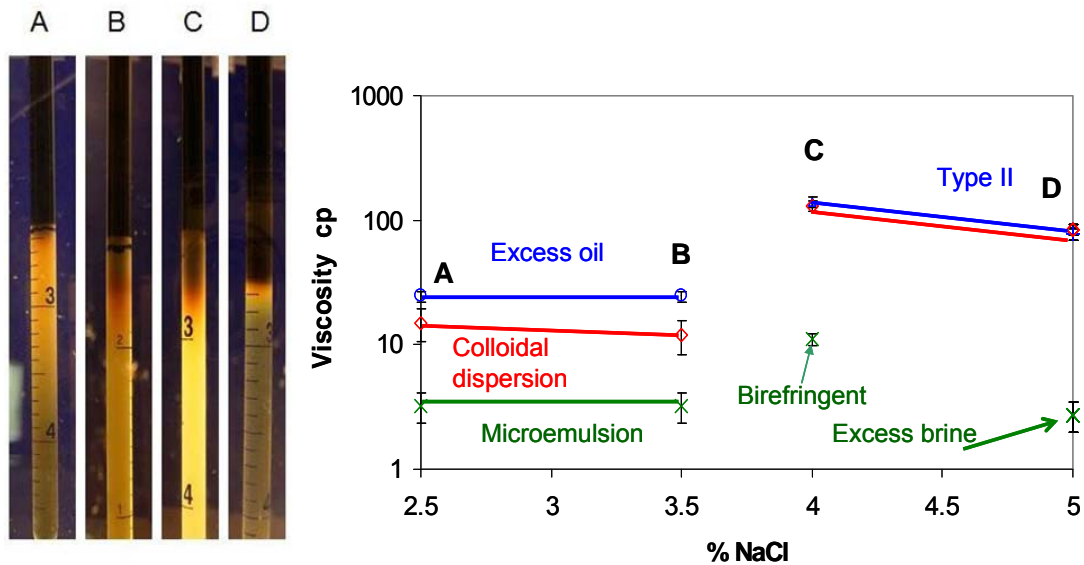


Fig. 9 Viscosity vs. % NaCl from a salinity scan test of a crude oil (SMY), 0.885 g/cm^3 and 23 cp, using 1% surfactant mixture ($C_{16-17} - 7 \text{ PO SO}_4 / \text{Internal olefin sulfonate } C_{15-18} : 4/1$) and $WOR=1$. Blue line represents the upper phase, red line is the average viscosity of the zone immediately below upper phase, and the green line represents the viscosity of lower phase.

In the Fig. 9 optimal conditions were found close to sample C. Lower phase of sample C exhibited birefringence and a viscosity three times higher than the microemulsions in samples A and B. Fig. 9 also shows that some formulations of surfactant at overoptimum conditions yield undesirable highly viscous phases or emulsions. Colloidal dispersion (Liu *et al.* 2008a, 2008b) layer had an intermediate viscosity between that of the upper and lower phases.

CONCLUSIONS

The falling sphere viscometer is able to measure viscosities ranging from 1 cp to 1,200 cp at ambient temperature. Viscosity of opaque phases or emulsions in sealed vials or pipettes in crude oil/brine/surfactant systems can be measured because the device uses inductive proximity sensors. Hence, the presence of undesirable highly viscous phases or emulsions can be detected and their potential adverse effects assessed. Previously such liquid crystals, condensed phases and emulsions could be identified only qualitatively by tilting the pipettes.

When the same phase spans the space between a pair of sensors, its viscosity can be estimated directly from the transit time of the sphere.

Viscosity of a middle-phase microemulsion can also be estimated even if it spans only a small fraction of the distance between sensors if viscosities of the upper and lower phases are measured either in the device itself or separately.

Apparent viscosities of macroemulsions and of the “colloidal dispersion” layer at the top of a lower-phase microemulsion have been measured (see Fig. 9).

NOMENCLATURE

A_F = Projected area (perpendicular to the velocity)

C_D = Drag coefficient.

$$C_D = \frac{F_D}{\frac{1}{2} A_F \rho U^2}$$

D_p = Particle diameter (sphere diameter)

D_c = Diameter of the pipette (internal diameter)

f = Correction to the drag coefficient for wall effects

F_D = Drag force.

g = gravity field (9.80665 m/s²)

K_1 = Wall effects, f

K_2 = Inertial effects

L_{TypeIII} = height of middle phase, m

N_{Ar} = Archimedes number.

$$N_{Ar} = \frac{\rho (\rho_s - \rho) g D_p^3}{\mu^2}$$

N_{Re} = Reynolds number for a particle (sphere)

$$N_{Re} = \frac{\rho U D_p}{\mu}$$

S_i = Sensor “i” (i=1,2,3,4)

U = Terminal velocity.

U_D = Dimensionless velocity

$$U_D = \frac{U}{\sqrt{gD_p}}$$

$V_p=V_s$ =Particle volume (sphere volume)

WOR_v = Volumetric water oil ratio

Greek symbols:

$\alpha = (\rho_s - \rho) / \rho_s$

$\beta = D_p / D_c =$ diameter ratio

$\beta_D = (3/4) (\rho / \rho_s)$

$$\gamma = \sqrt{\frac{\rho^2 D_p^3 g}{\mu^2}}$$

$\Delta\rho$ = Density difference.

$$\Delta\rho = |\rho_s - \rho|$$

Δx_1 = separation between sensors in the upper phase, m

Δx_2 = separation between sensors in the middle phase, m

Δx_3 = separation between sensors in the lower phase, m

Δx_4 = height from base to the first sensor, m

ΔL_u = Distance between the middle of sensor 2 and the interface between the upper phase and the middle phase

ΔL_L = Distance between the middle of sensor 3 and the interface between the lower phase and the middle phase

μ = Fluid viscosity.

ρ = Fluid density.

ρ_s = Solid density (sphere density)

θ = Dimensionless time

$$\theta = \frac{t}{\sqrt{D_p / g}}$$

Additional symbols, acronyms and abbreviations:

(C12OXS) = C₁₂-ortho-xylene-sulfonate

EO = ethylene oxide group, - (CH₂CH₂O)-

EOR = Enhanced Oil Recovery

n-C_m = normal alkane with m carbons

nEO = polyethylene oxide group, - (CH₂CH₂O)_n-

nPO = polypropylene oxide group, - (C₃H₆O)_n-

PO = propylene oxide group, - (C₃H₆O)-

SO₃ = Sulfonate group

SO₄ = Sulfate group,

tAA = tertiary amyl alcohol

Type I, II, III = Microemulsions Type I, II, III respectively using Winsor classification. (I=Oil in water, II = Water in oil, III=middle phase microemulsion)

1 cp=0.001 Pa s = 1 centipoise

Brookfield (DV-III Rheometer)= Couette flow viscometer

Ostwald. Cannon (IC 400-899D)= Capillary viscometer

Ostwald. Cannon (IC 200-y830)= Capillary viscometer

ACKNOWLEDGEMENTS

This research was supported by Chevron Energy Technology Company. We also gratefully acknowledge the support of Roberto Rocca Education Program and Tecnológico de Monterrey through the Research Chair in Solar Energy and Thermal-Fluid Sciences (Grant CAT-125).

REFERNCES

- Bennett K.E. , Macosko C.W. , Scriven L.E. Microemulsion Rheology Newtonian and Non-Newtonian Regimes. 1981, Paper *SPE* 10061 presented at the 56th ATCE of SPE , San Antonio, Texas, October 5-7, 1981
- Bennett K.E., Hatfield J.C., Davis H.T., Macosko C.W. and Scriven L.E. Viscosity and Conductivity of microemulsions. September 15-16, 1980. Presented at the Industrial Sub-Committee of the Faraday Division of the Chem. Soc. Meeting on Microemulsions.
- Benton W.J. and Miller C.A. Lyotropic Liquid Crystalline Phases and Dispersions in Dilute Anionic Surfactant-Alcohol-Brine Systems. 1. Patterns of Phase Behavior. 1983, *Journal of Physical Chemistry*, (87): 4983-4991
- Chhabra R.P., Agarwal S, Chaudhary K. A note on wall effect on the terminal falling velocity of a sphere in quiescent Newtonian media in cylindrical tubes 2003, *Powder Technology* (129) : 53– 58
- Chhabra R.P. Bubbles, Drops, and Particles in Non-Newtonian Fluids. 2nd Edition Taylor and Francis, 2007. Ch3: 59-94
- Francis A.W. Wall Effect in Falling Ball Method for Viscosity, 1933, *Physics* (4) : 403-406,
- Hackett J.L. and Miller C.A.. Microemulsions to Liquid-Crystal Transition in Two Anionic Surfactant Systems. 1988, *SPE Reservoir Engineering*: 791-900
- Liu S, Li R, Miller C.A, Hirasaki G.J, Wide Range of Conditions for Good Recovery 2008, Paper *SPE 113936 MS* presented at the 2008 SPE/DOE Symposium on IOR Tulsa, 22-26 April.
- Liu S, Zhang D.L, Yan W, Puerto M, Hirasaki G.J, Miller C.A. Favorable Attributes of Alkaline-Surfactant-Polymer Flooding. 2008 *SPE Journal*. 13(1):5-16
- Reed R.L. and Healy R.N. Some physicochemical aspects of microemulsion flooding: a review. *Improved Oil Recovery by Surfactant and Polymer Flooding*. (Editors D.O. Shah and R.S. Schechter) Academic Press,(1977) :383-437
- Healy R.N. and Reed R.L. Physicochemical Aspects of Microemulsion Flooding. 1974, *SPEJ* 4583 14(5) :491-501
- Suffi G. Consider all the factors when selecting the proper inductive proximity sensor, 2000. *Electronic Design*, 48(9) : 107-112
- Thomas R.H. and Walters K. The Unsteady Motion of a Sphere in an Elastic-viscous Liquid. 1966, *Rheologica Acta*, Band 5, Heft I: 23-27
- Turton R. and Levenspiel O. A Short Note on the Drag Correlation for Spheres, 1986 *Powder Technology*, (47) : 83 – 86
- Wilkes, J. 2006 *Fluid Mechanics for Chemical Engineers*. Prentice Hall

BIBLIOGRAPHY

- Bryan W.L and Bryan J.M. Viscometer for in situ monitoring, 1993. US. Patent No. 5, 203,203
- Eguchi, Karino. Measurement of Rheologic Property of Blood by a Falling-Ball Blood Viscometer. 2008, *Annals of Biomedical Engineering*. 1-9
- Harrison D.E. and Gosser R.B. Viscosity Measuring Apparatus, 1968 US. Patent No. 3,368,391

Kim K.T. Viscometer, 1968, US. Patent No. 3,375,705

Jones J.H. Viscometer. 1966. US. Patent No. 3,240,053

McGinn J.N. and Thomas L. Precision viscometer timer control system, 1973. US. Patent No. 3,772,910

Symmers E.M. Viscometer, 1930. US Patent No. 1,780,952.

APPENDIX

Phase Scenarios

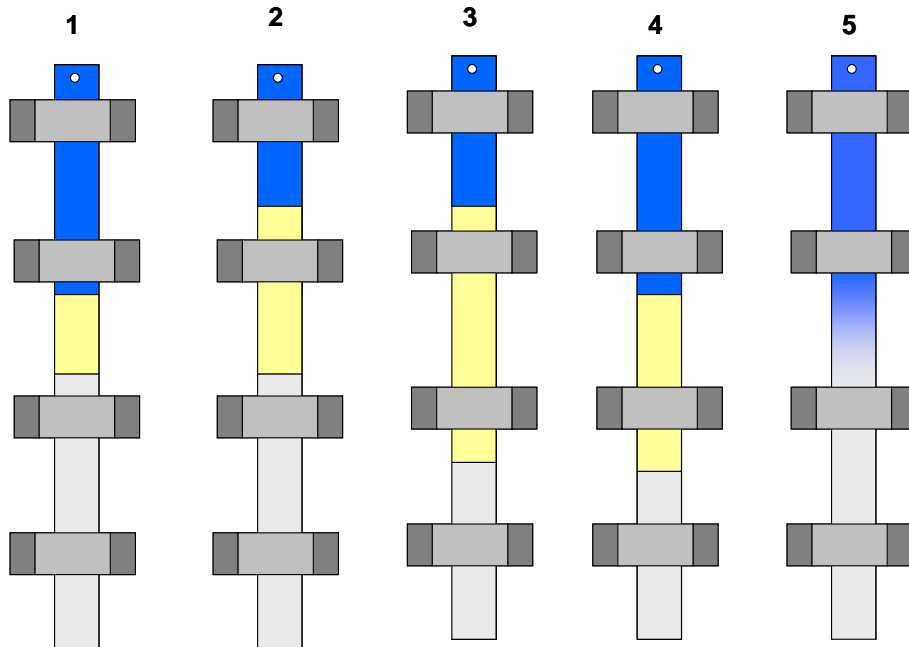


Fig A.1 Different scenarios to estimate the viscosity of different phases.

To determine the viscosity of different phases a MATLAB code was developed to consider five different scenarios shown in Fig A.1 and described below:

Scenario 1 : middle phase is between sensor 2 and 3

Scenario 2: middle phase is between sensor 1 and 3

Scenario 3: middle phase exceeds the depth of sensors 2 and 3

Scenario 4: middle phase is between sensor 2 and 4

Scenario 5: The measurement gives you the average viscosity of the fluid or mixture of fluids or phases between sensors.

To estimate the viscosity of the different phases it is recommended to position the pipette in the apparatus using the following criteria:

For upper phase Scenario 1 or 4 may be used. For lower phase scenario 1 or 2 may be used. For middle phase scenario 1 or 3 may be used. The sensors are located at fixed positions, but the pipette can be moved up-and-down to have these suggested scenarios. The MATLAB code can give an estimation of the viscosity of each phase subtracting times the sphere spends in the other phase, but

the user must be aware of transient effects. Transient effects are negligible only if the phase of interest has high viscosity.

Transients

To calculate the transients time to reach terminal velocity, a simple model of forces balances could be applied to solve the differential equations. These equations are given and were solved for different values of the parameters previously described in the Nomenclature Section. The dimensionless force balance is given in equation 6 (Wilkes, 2006):

$$\frac{dU_D}{d\theta} = \alpha - \beta_D U_D^2 C_D, \dots\dots\dots (6)$$

The drag coefficient given in equation (2), can be rearranged in the parameters shown in the differential equation:

$$C_D = \frac{24}{U_D \gamma} \left(1 + 0.173 (U_D \gamma)^{0.657} \right) + \frac{0.413}{1 + 16300 (U_D \gamma)^{-1.09}}, \dots\dots\dots (7)$$

The Archimedes number is related to the previous parameters (γ and β_D)

$$N_{Ar} = \gamma^2 \left(\frac{3}{4\beta_D} - 1 \right), \dots\dots\dots (8)$$

For a system with $\gamma=0.6$, and $\beta_D=0.08$, the time required to reach steady state starting at rest is 0.006s (in our systems analyzed the transient time was negligible in all the cases), the dimensionless time θ is less than 1, this result is consistent with more detailed analysis presented by Thomas et al. (1966)

Apparatus, materials and procedures.

Spheres

TABLE A1 Description of Spheres

| | |
|-----------------------------|---------------------|
| Manufacturer : CCR Products | www.ccrproducts.com |
| Model Number | SS440 CVM |
| Material | Stainless Steel |
| Size (in) | 1/32 |
| Grade | 3 |
| Lot No. | 29 |

Inductive ring sensors

Inductive proximity sensors are used to detect the falling sphere. These sensors detect metal by using resonance frequency electromagnetic fields. For the viscometer described here, Omron sensors and amplifiers are used.

TABLE A2 Table of specifications for sensor

| | |
|-------------------|-----------------------------|
| Manufacturer | OMRON |
| Model | F2LP-W10M |
| Price | \$103 each |
| Min Object Size | 0.3 dia. x 0.5 mm steel rod |
| Sensing Area (mm) | 10 dia. |
| Supplier | www.PLCcenter.com |

Amplifiers

TABLE A3 Table of specifications for amplifier

| | |
|--------------------------------------|----------------------|
| Table of Specification for Amplifier | |
| Manufacturer | OMRON |
| Model | F2LP-WK4 |
| Price | \$262 each |
| Supply Voltage | 120/240 VAC, 50/60HZ |
| Supplier | www.PLCcenter.com |

Software

All the programming for the falling-sphere viscometer is done using National Instrument's LabView software (version 8.2).

Data acquisition

All the parts making up the data acquisition system were purchased from National Instruments. Following is a table with a brief description of every part.

TABLE A4 Table of specifications for DAQ

| Part # | Description | Price |
|-----------|--|------------|
| 779694-01 | NI USB-6251 M SERIES DAQ DEVICE, MASS TERM, NI-DAQMX DRIVER, SIGNAL EXPRESS LE, US (120 V) | \$ 1214.10 |
| 778018-02 | SC-2345 WITH CONFIGURABLE CONNECTORS (FOR DAQPAD)-PWR02 | \$ 350.10 |
| 184749-01 | CABLE,TYPE SH68-68-EP, SHIELD CABLE,1 METER | \$ 89.10 |
| 777459-24 | SCC-AI05, 2-CHANNEL ISOLATED ANALOG INPUT | \$ 592.20 |

Procedures

Coating of spheres

Gold coating of the sphere is done using a bench-top sputter. Given that the coat can only be applied to the upper surface of the sphere, eight coats were applied to assure full coverage. A thirty-second coating can give a thickness of about 6 angstroms of gold.

When coating the spheres, one must assure maximum exposure by making sure that the spheres are not on top of each other or even right next to each other. This can be achieved by coating a small number of spheres at a time and shaking.

The bench-top sputter is available as shared equipment from Rice University's Chemistry department.

Sealing of the pipettes

Using an acetylene-oxygen torch, the pipettes were first sealed at the tip and subsequently at the top, after being previously filled with the test fluids and the paramagnetic ball inside. The samples that were prepared several years ago (see Fig. 7) were carefully open at the top with heat, the magnetic sphere inserted and then resealed. The serological glass pipettes were disposables from either KIMBLE (mL in 1/10) or FISHER (5 mL in 1/10).

Sample equilibration

The samples shown in Fig.6 and Fig.8 were left to equilibrate for a week before the pictures and their viscosity measurements were taken. The samples were not disturbed, and the different phases remained during the experiments. The samples in Fig.7 were equilibrated for more than 4 years and were not disturbed only by the paramagnetic ball during measurements. The samples in Fig.9 were equilibrated for approximated 1 ½ month.

Materials

Viscosity Standards

TABLE A5 Standard fluids used in the calibration of the falling sphere viscometer

| Fluid | Viscosity (cp) | Temperature (°C) | Lot number |
|-----------------------------------|----------------|------------------|-------------------|
| Brookfield viscosity standard 500 | 516 | 25 | 073101 |
| Brookfield viscosity standard 5 | 4.8 | 25 | 071201 |
| De-ionized Water 18.2 MΩ-cm | 0.89 | 25 | - |
| White mineral oil | 230 | 25 | MW ca. 540 g/gmol |

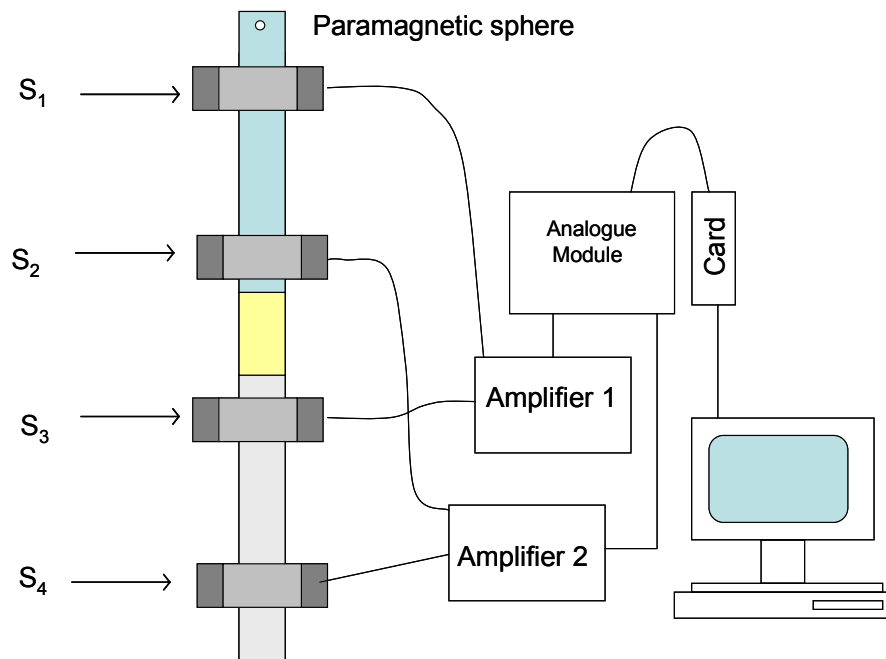


Figure A.2 The sensors and the amplifiers in the diagram are those described by TABLES A1 and A2. The DAQ of the computer, the analogue module, and the reading card.

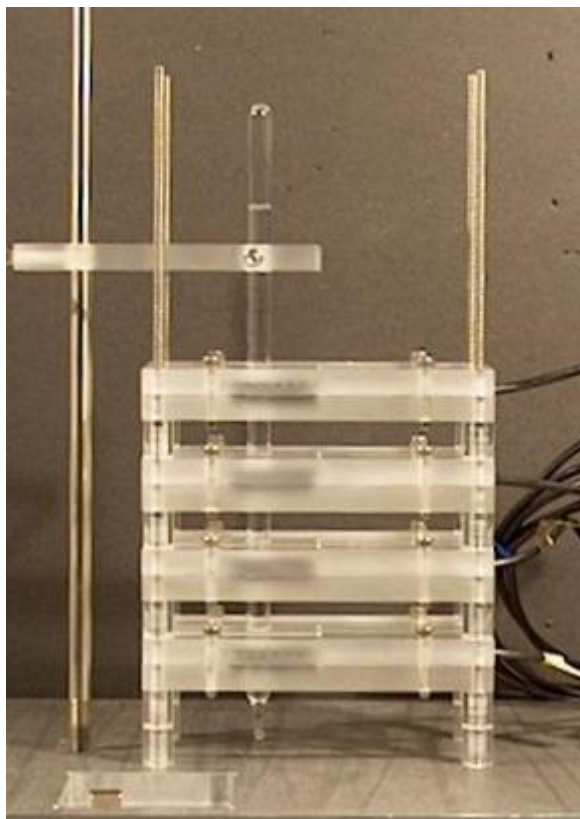


Figure A.3 Falling sphere viscometer with a sample

Jose Lopez-Salinas is a Ph D Graduate student in chemical and biomolecular engineering at Rice University. His research interests include interfacial science, porous media and enhanced oil recovery. He holds MS degree from ITESM Campus Monterrey, BS degree from Iniversidad Autonoma de Nuevo Leon, Mexico, both in Chemical Engineering. His is faculty at Monterrey Tec. **Kuy Koh Yoo** is undergraduate student at Rice University. **Maura C. Puerto** is a Complimentary Visiting Scholar at Rice University. She retired from ExxonMobil as a Research Associate after more than 25 years of service in the Reservoir Division. She holds a chemical engineering degree from Oriente University in Cuba. She was the recipient in 1980 of the SPE Cedric K. Ferguson Award, **George J. Hirasaki** had 26-year career with Shell Development and Shell Oil Companies before joining the Chemical Engineering faculty at Rice University in 1993. He was the 1999 recipient of the Society of Core Analysts Technical Achievement Award, and is a member of the National Academy of Engineers. He holds a BS degree in chemical engineering from Lamar University and a PhD degree in chemical engineering from Rice University. He received the SPE Lester Uren Award in 1989, and was named an improved Oil Recovery Pioneer at the 1998 SPE/DOR IOR Symposium. **Clarence A. Miller** is Louis Calder Professor of Chemical and Biomolecular Engineering at Rice University and a former chairman of the department. Before coming to Rice University, he taught at Carnegie-Mellon University. He has been a Visiting Scholar at Cambridge University, the University of Bayreuth (Germany), and the Delft University of Technology (Netherlands). His research interests center on emulsions, microemulsions, and foams and their applications in detergency enhanced oil recovery and aquifer remediation. He is coauthor of the book *Interfacial Phenomena*, the second edition of which was recently published by CRC Press. He hold BS and PhD degrees from Rice University and the University of Minnesota, both in chemical engineering.